Nanoscale

COMMUNICATION

View Article Online
View Journal | View Issue

Cite this: *Nanoscale*, 2024, **16**, 2877

Received 25th November 2023,
Accepted 7th January 2024

DOI: 10.1039/d3nr05989h

rsc.li/nanoscale

Nanogap engineering of 3D nanoraspberries into 2D plasmonic nanoclusters toward improved SERS performance†

Jian Yang, [a] Xinxing Zhang,[a] Lin Geng,[a] Chao Xia,[a] Xin Chen,[a] Wenzhong Yang,[a] Hui Xu *[a] and Zhiqun Lin *[b]

3D raspberry-like core/satellite nanostructures were prepared by controlled surface functionalization of silica spheres using crosslinked poly(4-vinylpyridine) (P4VP) chains with known binding affinity for gold nanoparticles (AuNPs). The 3D SiO_2-*g*-P(4VP-*co*-DVB)/AuNP nanoraspberries can be further transformed into 2D plasmonic nanoclusters by etching the silica core with hydrofluoric acid (HF). After the transformation, the interparticle distance between the AuNPs dramatically reduced from a 10 nm scale to sub 2 nm. Owing to the strong electromagnetic field generated by the plasmonic coupling between AuNPs in very close proximity, the established P(4VP-*co*-DVB)/AuNP nanoclusters provided strong and undisturbed Raman signals as a SERS substrate. In addition, benefiting from the stabilizing effect of the crosslinked P(4VP-*co*-DVB) network, the prepared SERS substrate has the advantages of good uniformity, stability and reproducibility, as well as strong SERS enhancement, endowing it with great potential for rapid and efficient SERS detection.

Surface-enhanced Raman scattering (SERS) is a powerful analytical technique that can amplify Raman scattering signals through analytes adsorbed on the surface of a material.[1,2] Over the past decades, SERS has achieved tremendous growth by virtue of fingerprinting, ultra-sensitive and nondestructive detection potential, and fast analytical capability without complicated sample pretreatment.[3,4] Therefore, this technology has been widely applied in various fields, including food,[5,6] environmental monitoring,[7,8] and chemical and biological sensing.[9,10]

Plasmonic metal nanoparticles (MNPs) have been utilized in SERS applications due to their unique wavelength-dependent surface plasmon resonance (SPR).[11–14] The SPR properties of plasmonic MNPs are mainly determined by the shape, size, and geometry of the nanoparticles. The electromagnetic field near plasmonic MNPs is generally localized in spatially narrow regions (so-called "hot-spots") in-between MNPs.[15–17] Therefore, the fabrication of SERS substrates with an enhanced electromagnetic field is of significant importance. Many reports have shown that the local electromagnetic coupling has strong sensitivity to the nanogap distance.[18–20] Therefore, the ability to control the interparticle distance of plasmonic MNPs offers the prospect to tune their optical properties for SERS applications.

When MNPs are utilized in SERS applications, the interparticle gap distance should be as short as a few nanometers to obtain strong Raman signals. Electron-beam lithography allows the design of ordered nanostructure arrangements with good reproducibility, but the minimum achievable gap between nanostructures is usually limited, typically to more than 10 nm.[21,22] The molecular-mediated assembly of MNPs has the potential to solve this problem by selecting bridging molecules that can fine-tune the interparticle spacing down to 1 nm.[23] However, these systems are usually sub-stable because of aggregation or dissociation.[24]

In recent years, 2D or 3D hierarchical MNP assemblies, such as nanocluster superstructures,[25–27] satellite structures,[28–30] and core–shell structures,[31,32] have been fabricated as SERS substrates due to the advantages of high-density hot spots. It was reported that MNP nanoclusters, such as gold NPs (AuNPs) and silver NPs (AgNPs), exhibited high SERS sensitivity with narrow nanogaps.[33–37] However, to fabricate nanoclusters that consist of closely packed MNPs is still quite challenging, due to the random aggregation issue and structural stability of the assemblies, which would result in non-uniform enhancement. In our previously reported work, we densely immobilized AuNPs on the surface of poly(4-vinylpyridine)-grafted carbon nanotubes (*i.e.*, CNT-*g*-P4VP) through Au–N interactions.[38,39] The P4VP brushes played an important stabilizing role in the immobilization of AuNPs on the support, *i.e.*, P4VP-grafted CNTs, which can effectively prevent the dissociation or coagulation of the AuNPs.

In this context, herein, for the first time, we propose a robust approach for fabricating P4VP-immobilized AuNP nano-

[a]*Institute of Advanced Synthesis, School of Chemistry and Molecular Engineering, Nanjing Tech University, Nanjing 211816, China. E-mail: ias_hxu@njtech.edu.cn*
[b]*Chemical and Biomolecular Engineering, National University of Singapore, 4 Engineering Drive 4, Singapore, 117585 Singapore. E-mail: z.lin@nus.edu.sg*
† Electronic supplementary information (ESI) available. See DOI: https://doi.org/10.1039/d3nr05989h

clusters as a SERS substrate. First, we employed divinylbenzene (DVB) as a cross-linking agent to graft a cross-linked P4VP shell onto SiO_2 nanospheres, resulting in the core–shell SiO_2-*g*-P(4VP-*co*-DVB). Then, the AuNPs were uniformly adsorbed onto the surface of SiO_2-*g*-P(4VP-*co*-DVB) to form 3D raspberry-like core/satellite SiO_2-*g*-P(4VP-*co*-DVB)/AuNP nanocomposites. Finally, tightly aggregated AuNP nanoclusters surrounded by cross-linked P(4VP-*co*-DVB) were obtained by etching the SiO_2 core with hydrofluoric acid (HF). It is a common belief that because of the random aggregation issue and structural stability of the assemblies, it is still quite challenging to fabricate nanoclusters with the interparticle spacing down to sub 2 nm. With our new concept, this method leads to plenty of highly regular 2D nanoclusters containing predominantly 150–200 AuNPs, with an average interparticle distance of sub 2 nm. The closely packed AuNPs provide effective interparticle coupling to generate abundant electromagnetic hot spots for application in SERS. Furthermore, the as-prepared SERS substrate shows high SERS activity for detection of organic molecules.

A schematic illustration for the fabrication of the SiO_2-*g*-P(4VP-*co*-DVB)/AuNP nanoraspberry and P(4VP-*co*-DVB)/AuNP nanocluster is depicted in Fig. 1. First, SiO_2-*g*-P(4VP-*co*-DVB) was prepared by introducing a small amount of cross-linker DVB, according to our previously reported route.[40] The SiO_2 nanosphere was covered with a slightly cross-linked thin P4VP shell. Then, SiO_2-*g*-P(4VP-*co*-DVB) can act as a template for the adsorption of AuNPs because the pyridine groups of P4VP can strongly bind with AuNPs through specific Au–N interactions. Finally, the SiO_2 core was etched using volatile HF vapor in a closed system, resulting in the P(4VP-*co*-DVB)/AuNP nanocluster.

As shown in Fig. 2, the materials were imaged by TEM and SEM at each step. The bare silica nanospheres have a smooth surface with an average diameter of ~200 nm (Fig. 2a). After grafting P(4VP-*co*-DVB) onto the surface of silica by ATRP, the core–shell nanostructure can be clearly observed (Fig. 2b).

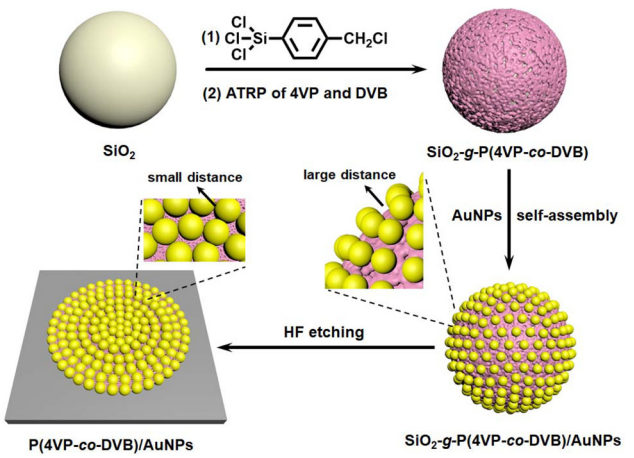

Fig. 1 Synthetic route to the SiO_2-*g*-P(4VP-*co*-DVB)/AuNP nanoraspberry and P(4VP-*co*-DVB)/AuNP nanocluster.

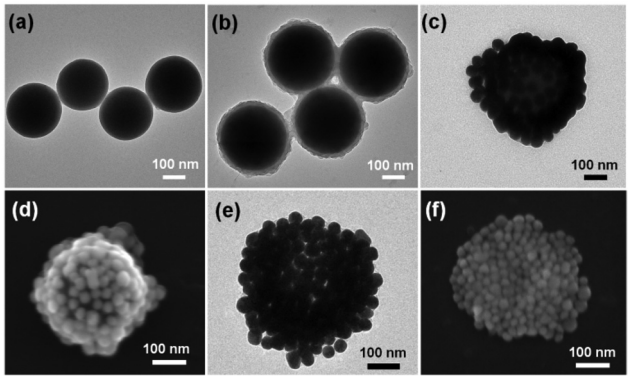

Fig. 2 TEM images of the (a) bare SiO_2 nanospheres, (b) SiO_2-*g*-P(4VP-*co*-DVB) core–shell nanostructure, (c) SiO_2-*g*-P(4VP-*co*-DVB)/AuNP nanoraspberry, and (e) P(4VP-*co*-DVB)/AuNP nanocluster. SEM images of the (d) SiO_2-*g*-P(4VP-*co*-DVB)/AuNP nanoraspberry and (f) P(4VP-*co*-DVB)/AuNP nanocluster.

TEM analysis confirmed that the thickness of the P(4VP-*co*-DVB) layer was ~20 nm. On the other hand, the size-stabilized AuNPs were synthesized by reducing aqueous $HAuCl_4$ solution with citric acid.[41] TEM analysis showed that the obtained AuNPs had an average size of 31.87 nm (Fig. S1†). The SiO_2-*g*-P(4VP-*co*-DVB)/AuNP nanoraspberries were obtained by adding an AuNP aqueous solution to a DMF solution containing dispersed SiO_2-*g*-P(4VP-*co*-DVB), followed by stirring for 5 min. The 3D raspberry-like nanoaggregate was obtained as shown in the TEM image (Fig. 2c). It was also clearly observed in the SEM image that the AuNPs were uniformly and densely adsorbed on the surface of the SiO_2-*g*-P(4VP-*co*-DVB) sphere (Fig. 2d). The P(4VP-*co*-DVB)/AuNP nanocluster was obtained by etching the SiO_2 core using HF vapor. Because of the disappearance of the SiO_2 support, the dispossessed AuNPs settled down into a closely packed aggregate structure due to gravity, which was imaged by TEM and SEM (Fig. 2e and f). The 3D spherical architecture of the SiO_2-*g*-P(4VP-*co*-DVB)/AuNP nanoraspberry transformed into a 2D planar structure of the P(4VP-*co*-DVB)/AuNP nanocluster. In addition, an obvious increase in the overall diameter of the AuNP aggregated structure was observed, from ~230 nm to ~350 nm. It should be noted that the AuNPs did not disperse randomly after etching SiO_2, but kept their regular circular aggregate structure. It can be attributed to the strong binding interaction of P4VP chains on AuNPs, which provides an effective stabilizing effect. This specific stable structure plays a crucial role in the following SERS detection study. Low magnification TEM and SEM images of the P(4VP-*co*-DVB)/AuNP nanoclusters are shown in Fig. S2 and S3,† respectively. The average size of the nanoclusters is estimated to be 0.51 μm (Fig. S3†).

To further investigate the heterostructures of the 3D SiO_2-*g*-P(4VP-*co*-DVB)/AuNP nanoraspberry and 2D P(4VP-*co*-DVB)/AuNP nanocluster, AFM measurements were also performed to characterize their height profiles (Fig. S4†). The AFM image showed an average height of 240 nm for the SiO_2-*g*-P(4VP-*co*-DVB)/AuNP nanoraspberry. It is reasonable that there is a

slight increase in height after loading the AuNPs, compared to bare AuNPs. After etching using HF, a dramatic decrease in height was clearly observed, due to the disappearance of the SiO_2 core. As for the P(4VP-*co*-DVB)/AuNP nanocluster, the average height of ~78 nm is about 2–3 layers of AuNPs. It is worth mentioning that owing to the strong adsorption behavior of P4VP on AuNPs, the AuNPs do not disperse and still maintain a regular circular aggregated structure, which corresponds well with the morphology shown by TEM in Fig. 2e.

The UV-Vis absorption spectra of the prepared bare AuNPs, SiO_2-*g*-P(4VP-*co*-DVB)/AuNPs and P(4VP-*co*-DVB)/AuNPs were measured. As shown in Fig. 3, the localized surface plasmon resonance (LSPR) absorption band of the bare AuNPs with an average diameter of 31.87 nm was centered at 528 nm (black line), and the LSPR absorption band of the SiO_2-*g*-P(4VP-*co*-DVB)/AuNPs was significantly red-shifted to 730 nm (red line), which is due to the interparticle plasma coupling of adjacent AuNPs stabilized on silica. The LSPR absorption band of the P(4VP-*co*-DVB)/AuNP composites, on the other hand, is red-shifted to 804 nm (blue line). Compared to that of the SiO_2-*g*-P(4VP-*co*-DVB)/AuNP nanoraspberries, the further red shift of the LSPR absorption band of the P(4VP-*co*-DVB)/AuNP nanoclusters should be attributed to the closer stacking of AuNPs after etching of the SiO_2, resulting in enhanced interparticle plasma coupling of adjacent AuNPs. It was found that the SiO_2-*g*-P(4VP-*co*-DVB)/AuNPs and P(4VP-*co*-DVB)/AuNPs show much wider LSPR absorption bands than pure AuNPs, which is attributed to the different interparticle nanogaps of adjacent AuNPs, resulting in varied plasma coupling strengths between AuNPs.

The effect of the prepared SiO_2-*g*-P(4VP-*co*-DVB)/AuNPs and P(4VP-*co*-DVB)/AuNPs on SERS detection was investigated using 4-MBA as a probe molecule. The SERS performance of bare AuNPs, SiO_2-*g*-P(4VP-*co*-DVB)/AuNPs and P(4VP-*co*-DVB)/AuNPs was evaluated by labeling the same concentration of 4-MBA (1.0 mM). As shown in Fig. S6a,† all three materials exhibited two characteristic peaks at 1077 and 1585 cm^{-1}, corresponding to the vibration of the 4-MBA benzene ring. In terms of the intensity, the pure AuNPs show a very low SERS signal. The SiO_2-*g*-P(4VP-*co*-DVB)/AuNPs can show an increased Raman signal due to the plasma coupling effect between adjacent AuNPs on SiO_2. Since pure AuNPs have a negative charge on their surface, the particles repel each other in solution. As a large number of AuNPs were immobilized on the SiO_2-*g*-P(4VP-*co*-DVB) surface, the AuNPs are in close proximity to each other, resulting in the generation of a large number of hot spots. As we expected, the prepared SiO_2-*g*-P(4VP-*co*-DVB)/AuNPs can be used as active SERS substrates. The large number of AuNPs on the surface of SiO_2-*g*-P(4VP-*co*-DVB) provides an available location for generating a large number of "hot spots", which can enhance the Raman signals. In addition, the 4-MBA molecule is easily attracted by the pyridine group of P4VP grafted on the surface of SiO_2-*g*-P(4VP-*co*-DVB) through hydrogen bonding, so the concentration of 4-MBA is enriched around SiO_2-*g*-P(4VP-*co*-DVB).[39] Quite intriguingly, it is obvious to find that the etched P(4VP-*co*-DVB)/AuNPs have a stronger signal than SiO_2-*g*-P(4VP-*co*-DVB)/AuNPs. After etching the silica core using HF, the satellite AuNPs immobilized by the P(4VP-*co*-DVB) shell settle into a planar architecture, allowing much tighter packing of the AuNPs. These intimate aggregations may trigger a higher SERS response because of the strong electromagnetic interactions between closer AuNPs.

In order to confirm that the SERS performance is dominated by the spacing of AuNPs in our study, we quantitatively measured the distances between the neighboring AuNPs before and after etching from the TEM results. The measurement method of the gap distance is according to the reported work by Bukasov *et al.*[42] Ten nanoaggregates were taken for the measurement of interparticle spacing. For each nanoaggregate, 15 interparticle distances were taken and measured. It should be noted that in most cases, the AuNPs are in contact with each other, as shown in Fig. S5.† The representative high resolution TEM images of SiO_2-*g*-P(4VP-*co*-DVB)/AuNPs (Fig. S5a) and P(4VP-*co*-DVB)/AuNPs (Fig. S5b†) show a clear gap view where the gaps can be accurately measured (marked with the left arrow) and a tilted/obscure gap view (marked with the right arrow) where the gaps may not be reliably measured. Only the clear gap view images were used to calculate the average interparticle distance. The interparticle distances of neighboring AuNPs before and after etching SiO_2-*g*-P(4VP-*co*-DVB)/AuNPs are presented in Tables S1 and S2,† respectively. According to the calculations, the average gap distances of the SiO_2-*g*-P(4VP-*co*-DVB)/AuNPs and P(4VP-*co*-DVB)/AuNPs are estimated to be 11.65 nm and 1.73 nm, respectively. After the structure transformation from the 3D SiO_2-*g*-P(4VP-*co*-DVB)/AuNP nanoraspberry to the 2D P(4VP-*co*-DVB)/AuNP nanocluster, the average interparticle distance between the AuNPs dramatically reduced from a 10 nm scale to sub 2 nm. Much stronger electromagnetic fields are generated by the plasmonic coupling between the AuNPs in closer proximity. Therefore, the P(4VP-*co*-DVB)/AuNP nanoclusters exhibited much higher

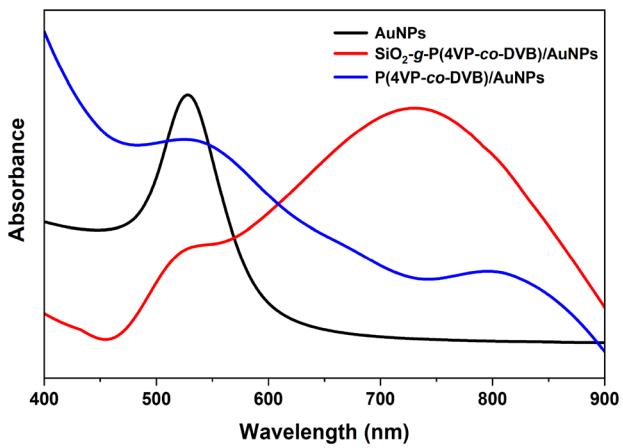

Fig. 3 UV-Vis absorption spectra of bare AuNPs (~31.87 nm) in aqueous solution (black line), and SiO_2-*g*-P(4VP-*co*-DVB)/AuNPs (red line) and P(4VP-*co*-DVB)/AuNPs (blue line) in the solid state.

Raman signals than the SiO_2-*g*-P(4VP-*co*-DVB)/AuNP nanoraspberries.

To further investigate the SERS performance of the P(4VP-*co*-DVB)/AuNP nanoclusters, typical SERS spectra of different concentrations of 4-MBA from 10^{-3} M to 10^{-12} M were recorded. As shown in Fig. 4a, the Raman intensity gradually decreased with the decrease of 4-MBA concentration. When the 4-MBA concentration was down to 10^{-11} M, we can still observe the two distinguishable peaks at 1077 and 1585 cm^{-1}. Therefore, the analyte detection limit can be as low as 10^{-11} M. As depicted in Fig. 4b, a linear curve was established by plotting the intensity of SERS signals at 1077 cm^{-1} against the concentrations of 4-MBA ranging from 10^{-3} to 10^{-12} M. The linear equation was calculated as $y = 4920.73x + 54\,112.6$ with an R^2 of 0.9921, showing a good linear relationship.

To determine and compare the enhancement factor (EF) of the prepared SiO_2-*g*-P(4VP-*co*-DVB)/AuNP nanoraspberry and P(4VP-*co*-DVB)/AuNP nanocluster as SERS substrates, they were uniformly deposited on silicon plates, respectively. As shown in Fig. S7,† two evenly distributed SERS substrates are obtained. Their EF values are estimated from eqn (S1).† The EF value of the SiO_2-*g*-P(4VP-*co*-DVB)/AuNPs was calculated to be 3.65×10^4, and that of the P(4VP-*co*-DVB)/AuNPs was 1.42×10^7. From the EF calculations, it can be deduced that the 2D P(4VP-*co*-DVB)/AuNP nanocluster showed a much stronger SERS response than the 3D raspberry-like SiO_2-*g*-P(4VP-*co*-DVB)/AuNPs. The SERS performance of the 2D P(4VP-*co*-DVB)/AuNP nanocluster was compared with that of the related materials reported in other published studies, as presented in Table S3.† Apparently, the 2D P(4VP-*co*-DVB)/AuNP nanocluster exhibits a higher EF value than these related materials.

To evaluate the reproducibility of the P(4VP-*co*-DVB)/AuNP nanocluster as a SERS substrate, a mass of P(4VP-*co*-DVB)/AuNP nanoclusters were uniformly deposited on a silicon plate. 50 randomly selected SERS spectral positions under identical experimental conditions were collected, as shown in Fig. 5a. The relative standard deviation (RSD) of the Raman signals of the peak at 1077 cm^{-1} was calculated to be 9.49% (Fig. 5b). The small intensity variations of these randomly selected spots suggested the good reproducibility of the P(4VP-*co*-DVB)/AuNP nanocluster. To evaluate the stability of the P(4VP-*co*-DVB)/AuNP nanocluster as a SERS platform, the SERS spectra of P(4VP-*co*-DVB)/AuNPs labeled with 1.0 mM 4-MBA were tested over a long period of time. The Raman signals of the P(4VP-*co*-DVB)/AuNP nanocluster were examined at monthly intervals. No significant decrease in SERS performance was found during a 3-month period (Fig. S8†). This indicates that the prepared P(4VP-*co*-DVB)/AuNP nanocluster has excellent stability.

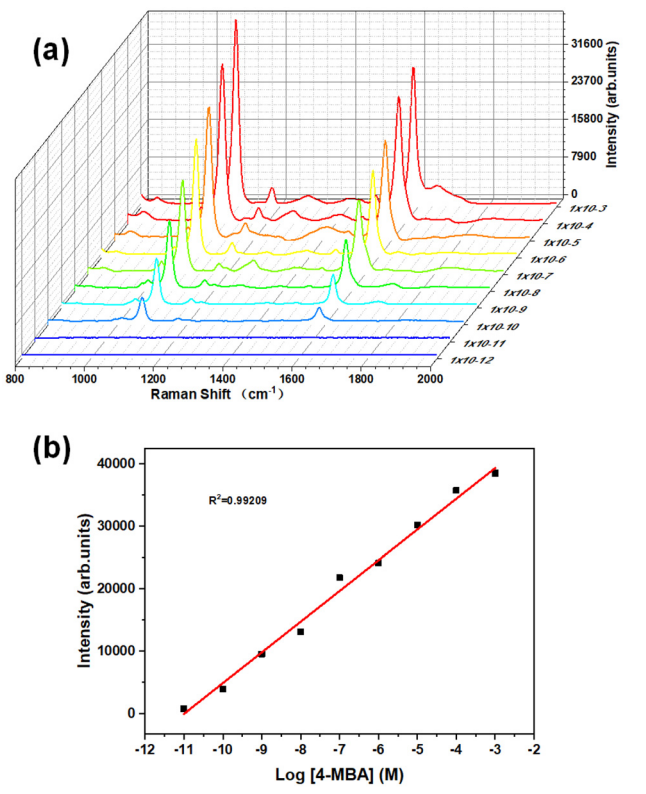

Fig. 4 (a) SERS spectra recorded for the P(4VP-*co*-DVB)/AuNP nanoclusters incubated with 4-MBA from 10^{-3} M to 10^{-12} M. (b) Calibration curve of the intensity of SERS signals at 1077 cm^{-1} *versus* the logarithm of 4-MBA concentration.

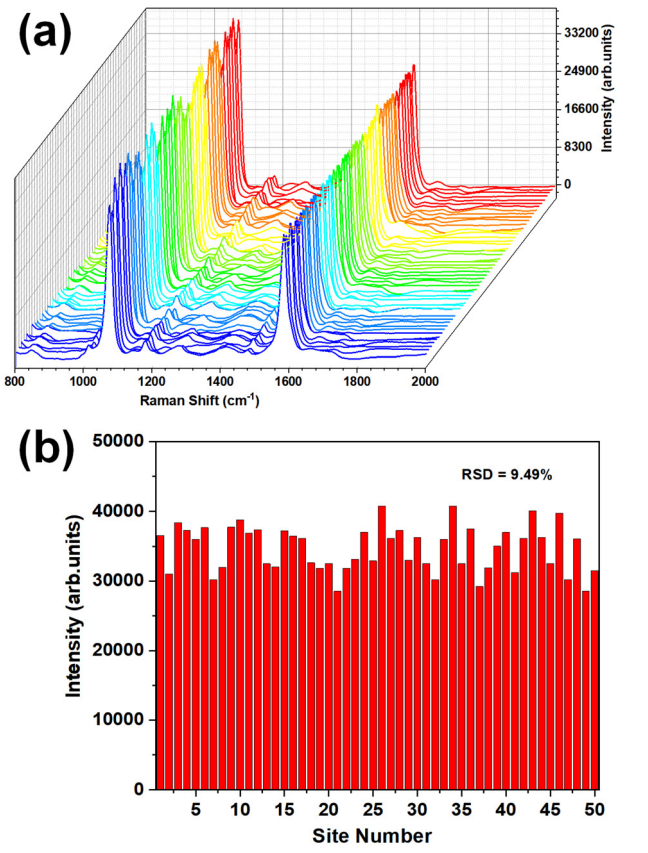

Fig. 5 (a) SERS spectra collected from 50 randomly selected spots of the P(4VP-*co*-DVB)/AuNP nanoclusters uniformly deposited on a silicon plate and (b) their corresponding variations of the intensities at 1077 cm^{-1}.

With the abuse of organic substances, the ecosystem is contaminated by their excessive residues in the aquatic environment. Therefore, it is of great importance to achieve sensitive detection of organic pollutants, such as dyes, pesticides and antibiotics in water. To evaluate the practical application of the P(4VP-*co*-DVB)/AuNP nanocluster as a SERS substrate in the field of organic pollutant detection, malachite green (MG) was employed as a target molecule. The SERS spectra of 1.0 mM MG aqueous solution adsorbed on the P(4VP-*co*-DVB)/AuNP nanocluster substrate were recorded as shown in Fig. S6b.† The major distinct Raman peaks in the SERS spectrum of MG are clearly observed, which are consistent with the results reported in the literature.[43,44] We also conducted SERS signal detection for four other organic pollutants, including thiram, crystal violet, ciprofloxacin and sulfamonomethoxine. Due to their unique molecular structures, the four substances exhibit fingerprint-like SERS spectra with distinct Raman peaks (Fig. S9†). Thus, the P(4VP-*co*-DVB)/AuNP nanocluster is proven to be a reliable SERS substrate for the sensitive detection of dyes, pesticides, and antibiotics.

Conclusions

In summary, we provide a facile and robust strategy to fabricate high SERS-responsive P(4VP-*co*-DVB)/AuNP nanoclusters. The synthetic process involves the immobilization of AuNPs on P4VP-grafted SiO_2, followed by HF etching to achieve the architecture transition from 3D nanoraspberries to 2D nanoclusters. TEM and SEM observations show that each 2D nanocluster consists of 150–200 closely packed AuNPs with an average interparticle gap of sub 2 nm, surrounded by cross-linked P(4VP-*co*-DVB) chains. The intimately aggregated AuNPs give rise to effective interparticle plasmon coupling, which generates abundant hot spots and provides strong SERS signals. The SERS performance tests of 4-MBA probe molecules indicate that the P(4VP-*co*-DVB)/AuNP nanoclusters are ultrasensitive SERS-active substrates with high stability and good reproducibility. Moreover, the P(4VP-*co*-DVB)/AuNP nanoclusters can serve as a useful SERS platform for rapid and efficient detection of dyes, pesticides, and antibiotics.

Author contributions

Jian Yang: data curation, formal analysis, visualization, and writing – original draft; Xinxing Zhang and Xin Chen: formal analysis and investigation; Chao Xia: investigation; Lin Geng: data analysis and validation; Wenzhong Yang: supervision; Hui Xu: conceptualization, supervision, funding acquisition, and writing – review & editing; Zhiqun Lin: writing – review & editing.

Conflicts of interest

There are no conflicts to declare.

Acknowledgements

The authors are grateful for the financial support from the National Natural Science Foundation of China (52002169), the Open Research Fund of State Key Laboratory of Organic Electronics and Information Displays (KL20210004), and the Nanjing Tech University Start-up Grant (39837122).

References

1 K. A. Willets and R. P. Van Duyne, *Annu. Rev. Phys. Chem.*, 2007, **58**, 267–297.
2 M. Moskovits and B. D. Piorek, *J. Raman Spectrosc.*, 2020, **52**, 279–284.
3 J. F. Li, Y. F. Huang, Y. Ding, Z. L. Yang, S. B. Li, X. S. Zhou, F. R. Fan, W. Zhang, Z. Y. Zhou, D. Y. Wu, B. Ren, Z. L. Wang and Z. Q. Tian, *Nature*, 2010, **464**, 392–395.
4 R. Pilot, R. Signorini, C. Durante, L. Orian, M. Bhamidipati and L. Fabris, *Biosensors*, 2019, **9**, 57.
5 C. Han, Y. Yao, W. Wang, L. Qu, L. Bradley, S. Sun and Y. Zhao, *Sens. Actuators, B*, 2017, **251**, 272–279.
6 D. Yang and Y. Ying, *Appl. Spectrosc. Rev.*, 2011, **46**, 539–560.
7 Y. Du, R. Liu, B. Liu, S. Wang, M. Y. Han and Z. Zhang, *Anal. Chem.*, 2013, **85**, 3160–3165.
8 L. B. Zhong, Q. Liu, P. Wu, Q. F. Niu, H. Zhang and Y. M. Zheng, *Environ. Sci. Technol.*, 2018, **52**, 5812–5820.
9 E. Garcia-Rico, R. A. Alvarez-Puebla and L. Guerrini, *Chem. Soc. Rev.*, 2018, **47**, 4909–4923.
10 C. Jiang, R. Liu, G. Han and Z. Zhang, *Chem. Commun.*, 2013, **49**, 6647–6649.
11 T. Itoh, M. Procházka, Z.-C. Dong, W. Ji, Y. S. Yamamoto, Y. Zhang and Y. Ozaki, *Chem. Rev.*, 2023, **123**, 1552–1634.
12 H. Lin, J. Mock, D. Smith, T. Gao and M. J. Sailor, *J. Phys. Chem. B*, 2004, **108**, 11654–11659.
13 P. L. Stiles, J. A. Dieringer, N. C. Shah and R. P. Van Duyne, *Annu. Rev. Anal. Chem.*, 2008, **1**, 601–626.
14 P. Yang, J. Zheng, Y. Xu, Q. Zhang and L. Jiang, *Adv. Mater.*, 2016, **28**, 10508–10517.
15 L. Litti and M. Meneghetti, *Phys. Chem. Chem. Phys.*, 2019, **21**, 15515–15522.
16 W. Ma, H. Kuang, L. Xu, L. Ding, C. Xu, L. Wang and N. A. Kotov, *Nat. Commun.*, 2013, **4**, 2689.
17 J. Li, K. M. Koo, Y. Wang and M. Trau, *Small*, 2019, **15**, 1904689.
18 N. J. Halas, S. Lal, W. S. Chang, S. Link and P. Nordlander, *Chem. Rev.*, 2011, **111**, 3913–3961.
19 S. L. Kleinman, R. R. Frontiera, A. I. Henry, J. A. Dieringer and R. P. Van Duyne, *Phys. Chem. Chem. Phys.*, 2013, **15**, 21–36.
20 K. A. Willets, *ChemPhysChem*, 2013, **14**, 3186–3195.
21 V. Merk, J. Kneipp and K. Leosson, *Adv. Opt. Mater.*, 2013, **1**, 313–318.
22 M. Kahraman, O. Aydin and M. Culha, *ChemPhysChem*, 2009, **10**, 537–542.

23 L. Guerrini and D. Graham, *Chem. Soc. Rev.*, 2012, **41**, 7085–7107.
24 S. Betelu, I. Tijunelyte, L. Boubekeur-Lecaque, I. Ignatiadis, J. Ibrahim, S. Gaboreau, C. Berho, T. Toury, E. Guenin, N. Lidgi-Guigui, N. Félidj, E. Rinnert and M. L. d. l. Chapelle, *J. Phys. Chem. C*, 2016, **120**, 18158–18166.
25 D. Bekana, R. Liu, M. Amde and J. F. Liu, *ACS Appl. Mater. Interfaces*, 2017, **9**, 513–520.
26 A. S. Urban, X. Shen, Y. Wang, N. Large, H. Wang, M. W. Knight, P. Nordlander, H. Chen and N. J. Halas, *Nano Lett.*, 2013, **13**, 4399–4403.
27 J. Xu, S. Huang, Z. Gao and Y. Song, *Chemosensors*, 2022, **10**, 442.
28 L. A. Wu, W. E. Li, D. Z. Lin and Y. F. Chen, *Sci. Rep.*, 2017, **7**, 13066.
29 R. P. M. Höller, M. Dulle, S. Thomä, M. Mayer, A. M. Steiner, S. Förster, A. Fery, C. Kuttner and M. Chanana, *ACS Nano*, 2016, **10**, 5740–5750.
30 S. A. Bethout, F. R. Baptista, S. J. Devereux, A. W. Parker, A. D. Ward and S. J. Quinn, *Nanoscale*, 2019, **11**, 19884–19894.
31 L. Sun, M. Zhang, V. Natarajan, X. Yu, X. Zhang and J. Zhan, *RSC Adv.*, 2017, **7**, 23866–23874.
32 Y. Lai, L. Dong, R. Liu, S. Lu, Z. He, W. Shan, F. Geng, Y. Q. Cai and J. F. Liu, *Chin. Chem. Lett.*, 2020, **31**, 2437–2441.
33 K. Kneipp, Y. Wang, H. Kneipp, L. T. Perelman, I. Itzkan, R. R. Dasari and M. S. Feld, *Phys. Rev. Lett.*, 1997, **78**, 1667–1670.
34 J. A. Dieringer, A. D. McFarland, N. C. Shah, D. A. Stuart, A. V. Whitney, C. R. Yonzon, M. A. Young, X. Zhang and R. P. Van Duyne, *Faraday Discuss.*, 2006, **132**, 9–26.
35 K. Sivashanmugan, J.-D. Liao, B. H. Liu, C.-K. Yao and S.-C. Luo, *Sens. Actuators, B*, 2015, **207**, 430–436.
36 T. Chung, T. Koker and F. Pinaud, *Small*, 2016, **12**, 5891–5901.
37 J. A. Fan, Y. He, K. Bao, C. H. Wu, J. M. Bao, N. B. Schade, V. N. Manoharan, G. Shvets, P. Nordlander, D. R. Liu and F. Capasso, *Nano Lett.*, 2011, **11**, 4859–4864.
38 H. Xu, Y. Sang, B. Xu, L. Zhang, L. Zhang and H. Xu, *ACS Appl. Nano Mater.*, 2020, **3**, 12169–12177.
39 R. Zhang, L. Geng, X. Zhang, Y. Sang and H. Xu, *Appl. Surf. Sci.*, 2022, **605**, 154737.
40 X. Chen, L. Zhang, B. Xu, T. Chen, L. Hu, W. Yao, M. Zhou and H. Xu, *Nanoscale Adv.*, 2021, **3**, 2879–2886.
41 B. V. Enustun and J. Turkevich, *J. Am. Chem. Soc.*, 1963, **85**, 3317–3328.
42 A. Arbuz, A. Sultangaziyev, A. Rapikov, Z. Kunushpayeva and R. Bukasov, *Nanoscale Adv.*, 2022, **4**, 268–280.
43 E. Ekmen, M. Bilici, E. Turan, U. Tamer and A. Zengin, *Sens. Actuators, B*, 2020, **325**, 128787.
44 L. B. Zhong, J. Yin, Y. M. Zheng, Q. Liu, X. X. Cheng and F. H. Luo, *Anal. Chem.*, 2014, **86**, 6262–6267.